Compact polymeric 3D prints of high stability

Goetz Peter Hellmann,[a] Christoph Kottlorz,[b] Jonas Presser,[c] and Katja Utaloff
Fraunhofer LBF, Darmstadt 64289, Germany

(Received 3 April 2014; accepted 6 June 2014)

The media advertizes that soon everybody can manufacture models and parts of all kinds via computer-aided design –computer-aided manufacturing by additive manufacturing (AM) technologies. That can boost the do-it-yourself activities enormously. But it can also revolutionize the industries: Most conventional technologies of manufacture are profitable only in big lots of production. For single specimens and small lots of production, they are too expensive. But with AM, one or a few original or spare parts can be produced at low cost. However, to succeed in the market, the AM products must become competitive. They must have reproducibility of an exact shape, even in tiny details, a perfect surface and, above all, sufficient mechanical strength. This article deals with three-dimensional ink-jet printing with monomer inks and polymer powders. Since powder beds are always porous, the main aim was to fill the pores permanently with high amounts of the ink polymer. A new polymer powder that rapidly dissolves in monomer inks is reported.

I. INTRODUCTION

Polymer parts are normally prepared by the technique of injection molding.[1] It is the basis of the success story of the polymers because it is fast, inexpensive, and well-developed. But it has one disadvantage: A metal mold, the negative of the part, into which the polymer melt can be injected, is needed for every newly designed part. That mold is too expensive for single parts and small production lots. But the demand of just those single parts and small production lots is rising, especially in branches as for instance medicine where tailor-made parts are needed.[2–4] To meet that demand, the additive manufacturing (AM) techniques are the only answer.[5–7]

The subject matter of this article is the three-dimensional (3D) ink-jet printing (3DP) of polymer parts where polymer powder layers are compacted successively by a computer-aided design (CAD)-guided ink jet.[8–10] Advantages of the 3DP method are that (i) it needs only a small and inexpensive apparatus similar to a two-dimensional (2D) printer, (ii) that multicolor is possible, and (iii) that no supporting structures need to be printed, since the surrounding powder acts as a support itself.

An important parameter in 3DP is the degree F to which the ink and its polymer fills the pores within the powder bed. In an ideal 3DP process, the ink fills all pores ($F = 100\%$), dissolves the powder grains and finally polymerizes. The end product is then compact, free of pores, and consists of the two polymers of the ink and the powder. These two must be compatible with one another. 3DP parts thus prepared may be able to compete with injection molding parts.

But this ideal is not yet the state of the art. So far, only small amounts of ink are used (*porous printing,* $F < 25\%$). This is not nearly enough to fill all pores in the powder bed. The ink swells the grains only superficially and glues them together locally (strategy I, Fig. 1). Therefore, the product is still almost as porous as the powder and extremely fragile. A posteriori, the pores are often filled with resins. But since these are usually very incompatible with the powder polymer, the thus modified products are still very brittle.[11] Currently, this is the most important disadvantage of the 3DP process.

By this description, porous printing strategy I seems quite useless. But it has an important merit: Small amounts of ink are easily retained due to the capillary forces in the powder bed. The ink does not leak into the surrounding powder, which allows an optimal reproduction of the shape given by the CAD model. The shrinkage during powder compaction is small enough, so that final dimensional errors are lower than 1%.[12]

In this article, attempts to come closer to the ideal (of producing an end product that is free of pores, consisting of just the two polymers the ink and the powder that are compatible with each other) are described. In all printing trials, larger amounts of ink were used, enough to fill most of the pores in the powder (*compact printing,* $F > 70\%$). The challenge was to optimize the dissolution of the powder grains by the ink.

[a]Address all correspondence to this author.
e-mail: g.hellmann@mc.tu-darmstadt.de
Present address: TU Darmstadt, Makromolekulare Chemie I, Darmstadt 64287, Germany
[b]Present address: Department Research & Development, Finma Chemie GmbH, Rosbach 61191, Germany
[c]Present address: Department Research & Development, Heidelberger Druckmaschinen AG, Heidelberg 69115, Germany
DOI: 10.1557/jmr.2014.137

 © Materials Research Society 2014

https://doi.org/10.1557/jmr.2014.137 Published online by Cambridge University Press

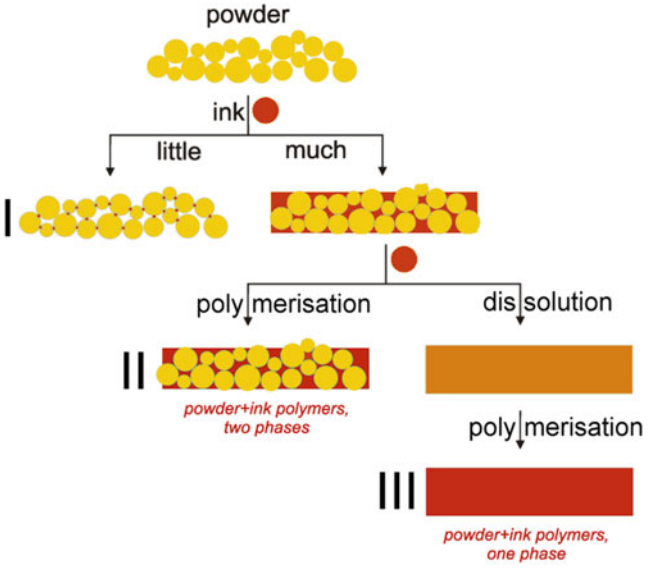


FIG. 1. Strategies of 3DP.

II. STRATEGIES

The preconditions of 3DP are

(i) The powder must flow freely under a doctor's knife or a roller to form smooth layers of >0.65 g/cm^3 density. The CAD-derived cross-sections are printed into them consecutively. Typical layer thicknesses vary between 70 and 150 μm. The grains should be spheres (beads) 5–150 μm in diameter. Irregularly shaped grains do not flow well. The powder layers are typically very porous. A good bed must have less than 50 vol% of pores.

(ii) The print head used (Spectra SL-128 AA, FUJIFILM Dimatix Inc., Santa Clara, CA) consisted of 128 individually controllable piezonozzles with an aperture diameter of 50 μm. The ink must leave the print head in drops with diameters $d \cong 50$ μm and it must not build satellite drops or strands. The printability of various inks can be determined by the characteristic number Z,[13–15]

$$Z = (\gamma \rho a)^{1/2} \Big/ \eta \geq 1 \qquad (1)$$

with γ the surface tension, η the viscosity, and ρ the density of the ink. The radius a of the nozzle aperture is set at 25 μm. Typically, inks with $1 < Z < 10$ show the best printability.[13,14] The ink can be a solvent which, however, will not be discussed in this article. In this study it always was a monomer. Hydroxyethyl methacrylate (HEMA, γ = 56 mN/m, η = 5 mPa, ρ = 1.07 g/cm^3) proved to be the most viable ink. With Z = 7.7, it formed clean drops and could be printed in reproducible amounts. HEMA could be polymerized radically within less than 15 min. To guarantee that this process starts exactly when the ink hits the powder, a two-component initiator system was used, comprising barbituric acid that was premixed with the powder and copper(II) ions dissolved in the ink.[16–18]

(iii) It is particularly important that the ink distributes controllably within the powder bed. The entire height of a print layer must be filled with the ink, so that the resulting monomer–polymer mixtures of successive print layers interdiffuse and form a stable connection. But the ink must not sag down from the layer actually being printed (printing layer) into lower layers. That destroys the precision of the print and overhangs as in a T-shaped part cannot be realized without bulges. Unfortunately, much ink as used in the compact printing aggravates the sagging. The ink runs through the printing layer down into the powder bed.

The steps of porous (I) and compact (II, III) printing are indicated in Fig. 1. The unwanted pores in products I are nicely filled in products II which consist of two polymers, that of the powder and that of the ink. However, the strategy II suffers badly from sagging of the ink before it is polymerized. That leads to strategy III where the ink dissolves the powder grains fast enough, at least partly, so a highly viscous, immobile polymer–monomer mixture results which is then solidified by polymerization of the ink. This is the strategy of choice on which this article is focused. The products III are homogeneous single-phase or compatible two-phase polymer–polymer solids.

III. PROCESSES AND PRODUCTS

The project was started with a commercial powder based on polymethyl methacrylate made by suspension polymerization[19] (S-PMMA, Fig. 2(a)) and an ink of HEMA which dissolves PMMA. The S-PMMA powder had a powder density of ρ_{powder} = 0.67 g/cm^3 and a grain size distribution shown in Fig. 2(b).

Porous printing (F = 22%) was easy with this S-PMMA powder. Figure 3 shows a porously printed test bar. The geometry of the CAD-model was correctly reproduced with sharp edges and corners.

But the S-PMMA powder did not at all permit compact printing. In Fig. 4, the print of three test bars as in Fig. 3 is shown, but this time with F = 84%. The ink did not stay in place but ran wildly through the printed powder and moreover leaked out into the surrounding powder. The individual test bars could not be isolated.

HEMA dissolved the S-PMMA beads well but way too slowly. The microscopic images in Fig. 5 show one original bead and the same bead after 5 h in HEMA. Even after 10 h, it was not completely dissolved. The time duration that the ink needed to diffuse into the grains was too long. The powder grains must dissolve in minutes, to thicken the ink efficiently. Consequently, a new powder, not yet in the market, was developed.

https://doi.org/10.1557/jmr.2014.137 Published online by Cambridge University Press

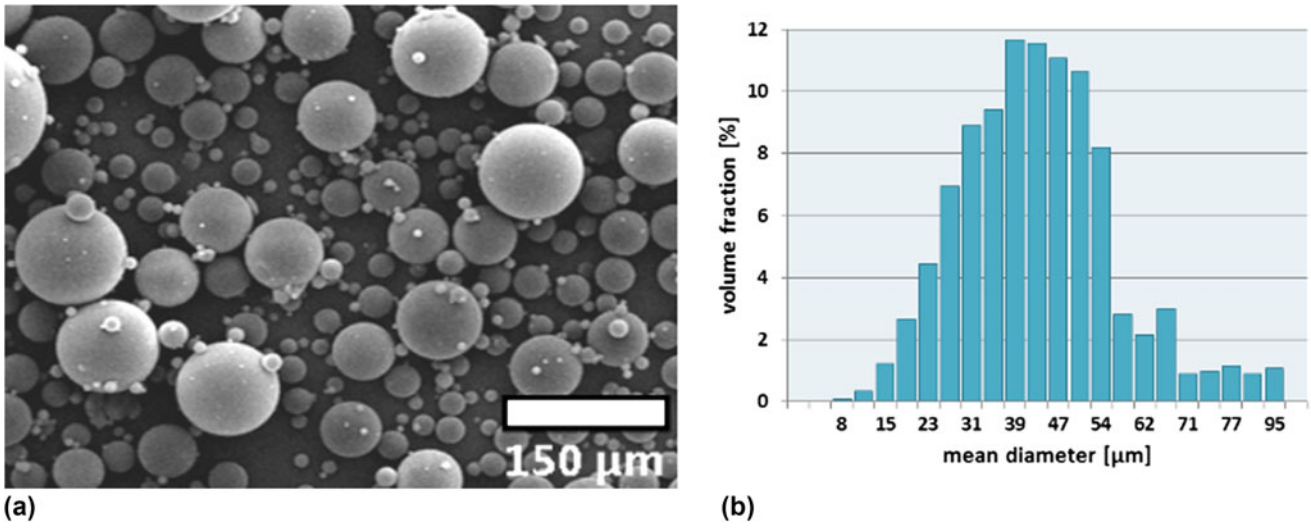


FIG. 2. S-PMMA powder: (a) powder beads, (b) grain size distribution.

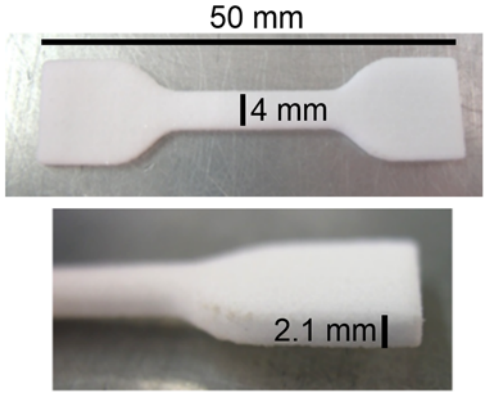


FIG. 3. State-of-the-art porous print (F = 22%).

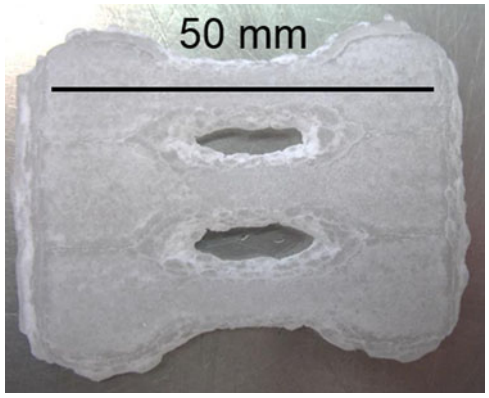


FIG. 4. Compact print with S-PMMA powder (F = 84%).

There are two reasons, why the S-PMMA was so hard to dissolve: First, the S-PMMA beads are monolithic, without any inner structure, so the beads can only be slowly dissolved from the outside. Second, PMMA has a high glass transition temperature of T_g = 120 °C and remains at room temperature a hard solid difficult to penetrate.

In the initial attempts, the bead size was lowered, but the resulting powders did not flow well anymore, due to the electrostatic attraction between the beads. Then, powders of other polyalkylmethacrylates with lower glass transition temperatures were tested, with grains as large as in S-PMMA. PethylMA with T_g = 76 °C was dissolved in 1 h and PbutylMA with T_g = 32 °C even in 10 min, fast enough for compact printing. But polymer beads with lower T_g tended to superficially stick to each other, resulting in insufficient flow properties and thus in highly porous powder beds.

Therefore, the internal structure of grains was changed, for facilitating the ink penetration. At first, powders with aggregate grains consisting of PMMA nanobeads were tried. But as those grains were not spherical, they did not yield good powder layers. Then, the PMMA was combined with another polymer, an elastomeric copolymer of MMA and butyl methacrylate (PMMA-co-PBA). That led to the microblend bead (MB). Its grains were prepared by a two-step suspension polymerization. The synthesis involved an incomplete polymerization of the monomer MMA to a PMMA–MMA mixture, followed by the addition of the monomer butyl acrylate (BA) and its polymerization together with the MMA to a copolymer PMMA-co-PBA. In the end, the grains of this MB powder consisted of a compatible polymer blend. The reaction steps are summarized in Fig. 6.

IV. EXPERIMENTAL

A. Materials

The monomers MMA and BA (Evonik) were destabilized with 1 N sodium hydroxide solution and dried over magnesium sulfate prior to use. HEMA (Aldrich),

https://doi.org/10.1557/jmr.2014.137 Published online by Cambridge University Press

dibenzoyl peroxide (DPO 25% water, Merck Millipore, Billerica, MA), copper(II) naphthenate (8% Cu, ABCR GmbH, Karlsruhe, Germany), 5-*n*-butyl(barbituric acid) (Chemische Fabrik Berg GmbH, Bitterfeld-Wolfen, Germany), and a poly(vinyl alcohol) surfactant POVAL KL-318 [25-88] (Kuraray Europe GmbH, Hattersheim am Main, Germany) were used as received. The commercial S-powder was received from Voxeljet AG, Germany.

B. MB powder synthesis

The MB powder was synthesized in a 1 L double-walled reactor equipped with a reflux condenser, nitrogen inlet, and a 6-hole paddle stirrer. An emulsion of 500 g water containing 5 g POVAL KL-318 [25-88] and 125 g of MMA, 1.25 g of dibenzoyl peroxide (DPO) (1 wt%) was stirred at 400 rpm at room temperature for 1 h and purged with nitrogen. Then the temperature was raised by an external thermostat to 75 °C and the monomer polymerized under nitrogen for 105 min. After this time, the conversion of MMA was $P = 30\%$. The thermostat was filled with ice and the reactor content was cooled to 25 °C, thus interrupting the polymerization. 62 g BA was mixed with 600 mg DPO and transferred to the reactor. The prepolymerized beads were swollen by the monomer over a period of 18 h at 45 °C. The polymerization was then continued at 75 °C under nitrogen for 4 h. The finished suspension was centrifuged, washed three times with water, and dried in an oven at 40 °C. Grain aggregates larger than 180 μm were removed by sieving.

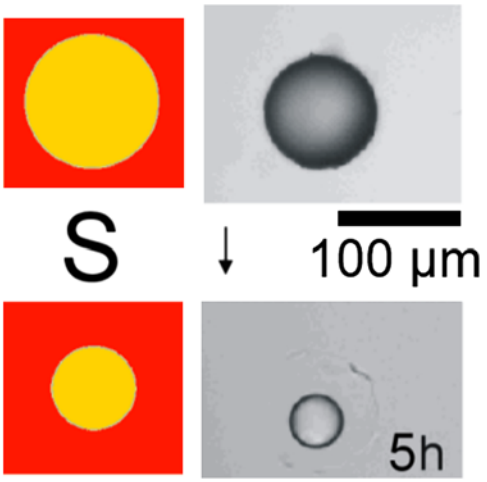


FIG. 5. Dissolution of a S-PMMA grain in HEMA.

C. 3DP

Prints were made on a VX testing-stand (Voxeljet AG, Germany) with an automated powder application, a powder roller, and a print head consisting of 128 individually controllable piezonozzles. The specimens for stress-strain measurements consisted of 14 layers with a layer thickness of 150 μm.

D. Polymerization

The polymerization of HEMA during the printing was activated by a two-component initiator system comprising 0.75 wt% 5-*n*-butyl(barbituric acid) that was premixed with the powder and 0.06 wt% copper(II) naphthenate that was dissolved in the ink. Once completed, the parts were heated in an oven for 6 h at 80 °C.

E. Dissolution test

To test the dissolution rate of the powder, single grains, approximately 100 μm in size, were covered with one drop of HEMA and the dissolution was monitored at room temperature with a light microscope Olympus BX50F (Olympus Europe GmbH, Hamburg, Germany). The software analySIS auto (Olympus) was used to control the recordings. Dissolution times were measured until the original bead was completely dissolved. The dissolution test of S-PMMA was stopped after 10 h.

F. Grain size distribution measurements

The size distributions were generated from light microscopic images (Olympus BX50F) of powder monolayers on glass slides. The powder grains were classified in their size and counted by the software analySIS auto (Olympus). A size distribution measurement consisted of at least 2000 measurement points.

G. Electron microscopy

Electron micrographs were taken with a scanning electron microscope (SEM; Model SM-300, TOPCON AG, Tokyo, Japan) and a transmission electron microscope (TEM; Model EM 902, Carl Zeiss AG, Oberkochen, Germany). Ultrathin sections were prepared on an ultramicrotome Ultracut UTC (Leica Mikrosysteme

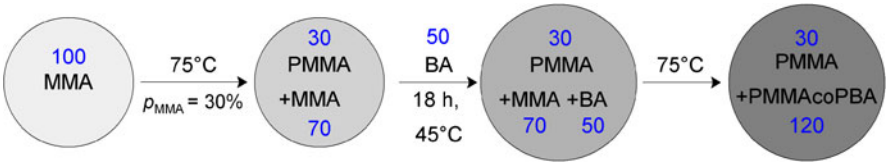


FIG. 6. Composition of the MB beads at different stages of the synthesis (wt%).

https://doi.org/10.1557/jmr.2014.137 Published online by Cambridge University Press

Vertrieb GmbH, Wetzlar, Germany). Powder grains were embedded in epoxy resin, trimmed with a diamond knife trimm 45 (DiAtome AG, Biel, Switzerland), and cut to 70- to 90-nm thin sections with a diamond knife Cryo 45 (DiAtome AG) at −50 °C.

H. Stress–strain measurements

The stress–strain measurements were recorded with a Zwicki-Line 2.5 kg (Zwick GmbH & Co. KG, Ulm, Germany). For every print trial, three printed test bars with a cross-section of 4 mm × 2.1 mm and an initial

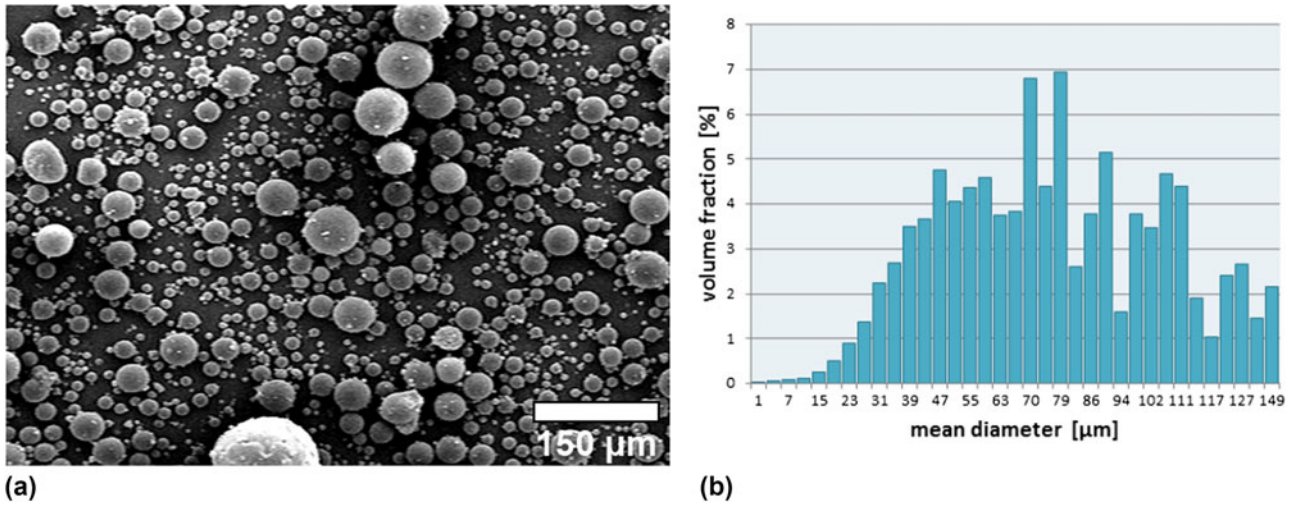


FIG. 7. MB powder: (a) powder beads, (b) grain size distribution.

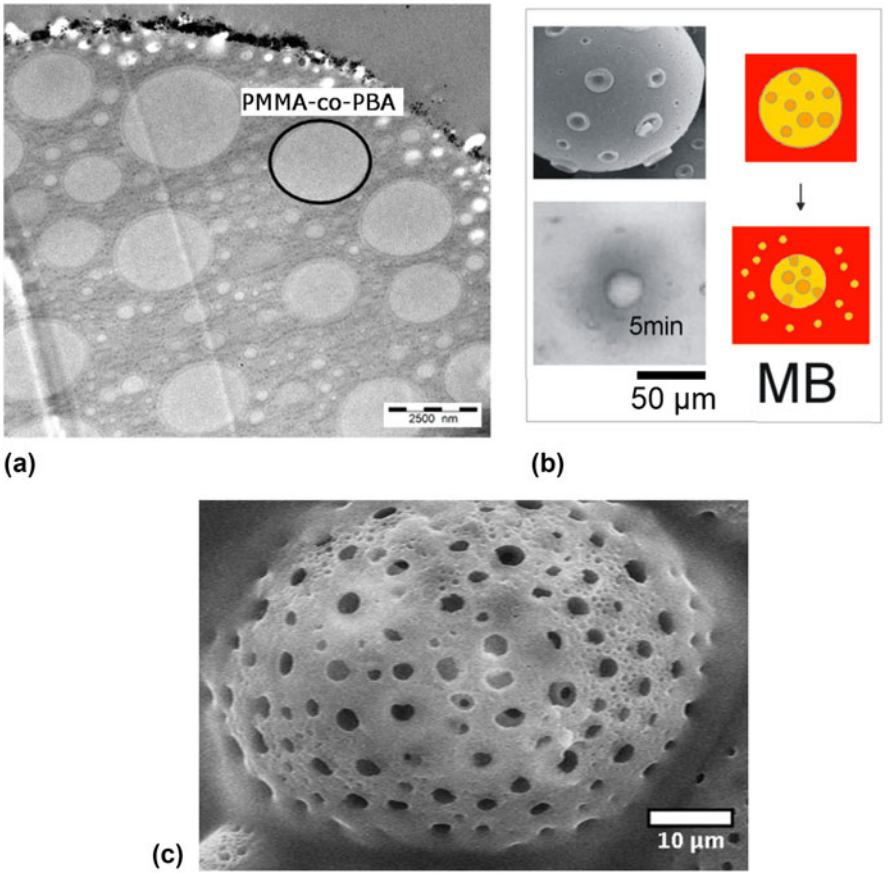


FIG. 8. MB suspension beads: (a) internal microblend structure (TEM), (b) dissolution in HEMA, (c) cage structure of the PMMA-matrix after extraction of the copolymer domains (SEM).

https://doi.org/10.1557/jmr.2014.137 Published online by Cambridge University Press

gauge length of 17 mm were elongated at a rate of 2 mm/min at 25 °C. The resulting stress versus strain curves were used to calculate tensile stress, stress at break, modulus of elasticity, and the percentage of elongation at break.

I. Powder density measurements

The measurements of the powder density were related to DIN ISO 697. The powder was poured from a funnel into a standard cup of known volume and weighed.

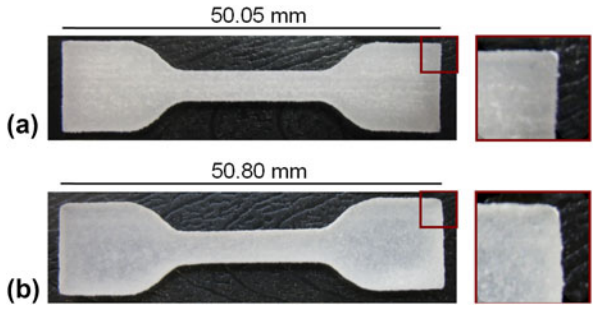


FIG. 9. 3DP product of the MB powder: (a) F = 53%, (b) F = 84%.

V. MICROBLEND POWDER CHARACTERISTICS AND 3D-PRINTED PARTS

The grains of the MB powder [Fig. 7(a)] consisted of PMMA and the copolymer PMMA-co-PBA. Compared with the grain size distribution of the S-PMMA [Fig. 2(b)], the MB powder had a broader size distribution with a higher content of beads smaller than 15 μm and larger than 100 μm. This resulted in a higher powder density of $\rho_{powder} = 0.71$ g/cm^3.

As shown in the magnification in Fig. 8, each grain had an internal structure of a hard, thermoplastic PMMA matrix (T_g = 120 °C) in which soft, elastomeric PMMA-co-PBA domains (T_g = 47 °C), more exactly $PMMA_{20}/(PMMA_{58}\text{-co-}PBA_{42})_{80}$ were dispersed. The surface of these grains was covered with PMMA. That ensured the good flow properties of the MB powder.

The soft copolymer domains had a huge impact on the dissolution behavior because they dissolved rapidly in the ink. In Fig. 8(b), a bead is shown in the dry state and after 5 min in HEMA. During that time the elastomeric domains were completely dissolved. Only a cage-like

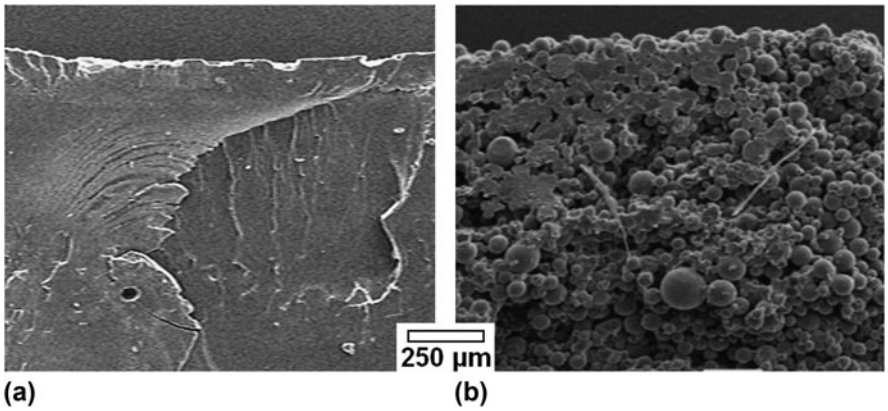


FIG. 10. Electromicrographs of cross-sections: (a) compact print with MB powder (F = 84%), (b) porous print with S-PMMA powder (F = 22%).

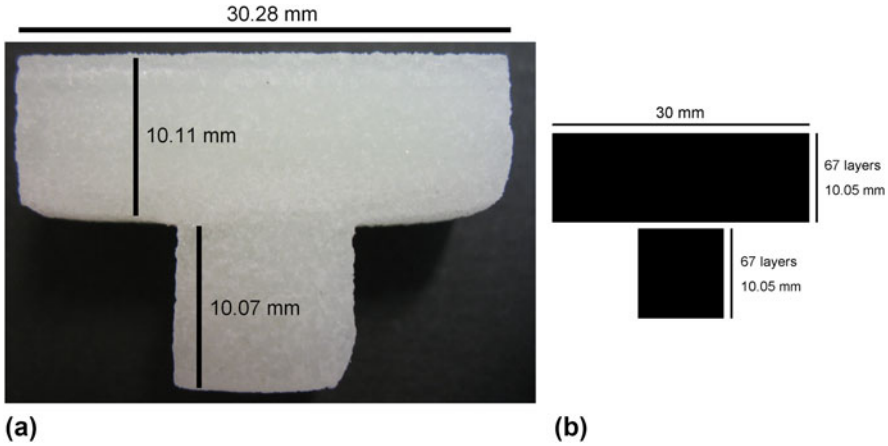


FIG. 11. T-shaped body printed with MB powder (F = 84%): (a) real dimensions, (b) ideal dimensions.

https://doi.org/10.1557/jmr.2014.137 Published online by Cambridge University Press

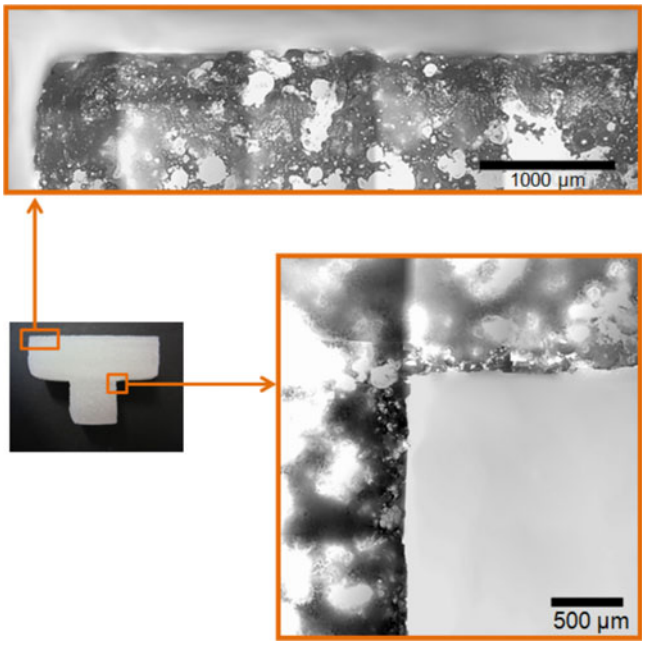


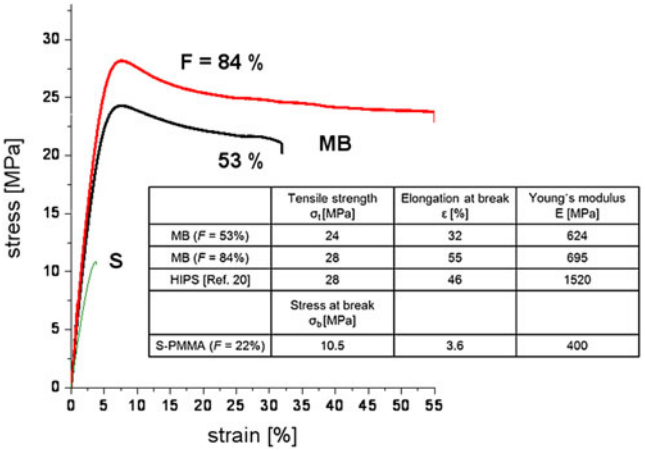
FIG. 12. Magnifications of the T-shaped body: upper edge and overhang.

structure of the hard PMMA matrix remained [Fig. 8(c)]. It dissolved entirely in another 10 min.

This MB powder could be 3D printed satisfactorily at various degrees F of pore filling. In Fig. 9, 3DP products with two degrees are shown (F = 53% and F = 84%). A comparison to the compact print with S-PMMA powder in Fig. 4 proves the ability of the MB powder to hold the ink in place and prevent its uncontrolled leakage. The three adjacently printed test bars no longer blended with each other. Edges and corners were surprisingly sharp. The quality was almost equal to that of the porously printed test bar in Fig. 3. Only at higher degrees F of pore filling [Fig. 9(b)] dimensional errors increased and corner sharpness decreased.

At F = 84%, the ink filled most of the pores in the powder. As witnessed by the electromicrograph in Fig. 10(a), the MB powder grains were completely dissolved by the ink and the resulting polymer blend was nearly free of pores. In comparison, the cross-section of a porously printed part in Fig. 10(b) was composed of individual beads that were bonded together only superficially.

To further test the sagging behavior of the ink, the T-shaped body in Fig. 11(a) was printed with F = 84%. The base was composed of 67 quadratic cross-sections, each 150-µm thick, and the overhang of 67 rectangular cross-sections [Fig. 11(b)]. The dimensional accuracy of the body suffered from still existing problems: Although the height was reproduced well, the overhang was too long, indicating that the ink was not yet held back perfectly. Also the body had two rounded corners on the right side. This, however, was not a problem of the high amount of ink, but a problem of the process technology.



	Tensile strength σ_t [MPa]	Elongation at break ε [%]	Young's modulus E [MPa]
MB (F = 53%)	24	32	624
MB (F = 84%)	28	55	695
HIPS [Ref. 20]	28	46	1520
	Stress at break σ_b [MPa]		
S-PMMA (F = 22%)	10.5	3.6	400

FIG. 13. Stress– strain curves and mechanical properties of test bars printed with S-PMMA powder and MB powder.

During the application of a new powder layer, the roller slightly compressed freshly printed layers that lay loosely on the powder.

But the T-shaped body also pointed out the advantage of the MB powder. The magnifications in Fig. 12 proved that the upper edge was very sharp, with an accuracy of ±50 µm. The same applied to the overhang that was completely free of bulges. Compact printing was possible without sagging of the ink.

The porous (S-PMMA) and compact (MB powder) test bars were subjected to stress–strain measurements (Fig. 13), to investigate the influence of the reduced porosity on the mechanical properties. The compact parts showed an improved tensile strength of up to 28 MPa as compared to 10.5 MPa of porous parts. Also the elastomeric domains within the MB powder grains had a significant influence: They made the printed products tough and impact resistant. The mechanical properties of compact parts with F = 84% are comparable to that of injection molded high-impact polystyrene.[20]

VI. CONCLUSION

3DP can become, in the family of the new AM methods, a member with a high potential. But it needs novel, better powders that guarantee competitive 3DP products. The MB powder in this study sets the foundation for a new, compact print strategy. It flows freely, is rapidly dissolved in monomer inks, can hold these inks and renders the 3DP parts impact-resistant. For further improving the dimensional accuracy of compact parts, future work will focus on adapting the printing technique of commercial 3D printers to this new material system.

ACKNOWLEDGMENTS

The authors would like to thank the "Arbeitsgemeinschaft industrieller Forschungsvereinigungen "Otto von Guericke" e.V. (AiF)" and the

https://doi.org/10.1557/jmr.2014.137 Published online by Cambridge University Press

"Bundesministerium für Wirtschaft und Energie (BMWi)" for the promotion of this project.

The IGF-project 17137 N of the research association "Kunststoffe" was promoted by the AiF under the program for the promotion of industrial research (IGF) by the "Bundesministerium für Wirtschaft und Energie", following a decision of the German Bundestag.

REFERENCES

1. M.R. Kamal, A.I. Isayev, and S. Liu: *Injection Molding Technology and Fundamentals* (Hanser Gardner Publ, Cincinnati, 2009).
2. A. Sridhar, D. Attanasio, and A. Nannini: Trends and expertise exchange within rapid manufacturing in Europe. *RTejournal* **7**, 1–12 (2010).
3. F. Rengier, A. Mehndiratta, H. von Tengg-Kobligk, C.M. Zechmann, R. Unterhinninghofen, H-U. Kauczor, and F.L. Giesel: 3D printing based on imaging data: Review of medical applications. *Int. J. Comput. Assist. Radiol. Surg.* **5**, 335–341 (2010).
4. A. Khalyfa, S. Vogt, J. Weisser, G. Grimm, A. Rechtenbach, W. Meyer, and M. Schnabelrauch: Development of a new calcium phosphate powder-binder system for the 3D printing of patient specific implants. *J. Mater. Sci.: Mater. Med.* **18**, 909–916 (2007).
5. N. Hopkins, R. Hague, and P. Dickens: *Rapid Manufacturing: An industrial Revolution for the Digital Age* (John Wiley & Sons, West Sussex, 2006).
6. X. Yan and P. Gu: A review of rapid prototyping technologies and systems. *Comput.-Aided Des.* **28**, 307–318 (1996).
7. P.A. Webb: A review of rapid prototyping (RP) techniques in the medical and biomedical sector. *J. Med. Eng. Technol.* **24**, 149–153 (2000).
8. E.M. Sachs, J.S. Haggerty, M.J. Cima, and P.A. Williams: Three-dimensional printing techniques. US Patent No. 5204055 (1993).
9. J. Bredt, S. Clark, W. Derek, and M. Dicologero: Thermoplastic powder material system for appearance models from 3D printing systems. WO 2004113042 (2004).
10. P. Patirupanusara, W. Suwanpreuk, T. Rubkumintara, and J. Suwanprateeb: Effect of binder content on the material properties of polymethyl methacrylate fabricated by three dimensional printing technique. *J. Mater. Process Technol.* **207**, 40–45 (2008).
11. B. Lozo, M. Stanic, S. Jamnicki, S.J. Poljacek, and T. Muck: Three-dimensional ink jet prints—impact of infiltrants. *J. Imaging Sci. Technol.* **52**, 51004 (1)-51004(8) (2008).
12. M. Salmi, K.S. Paloheimo, J. Tuomi, J. Wolff, and A. Mäkitie: Accuracy of medical models made by additive manufacturing (rapid manufacturing). *J. Craniomaxillofac. Surg.* **41**, 603–609 (2013).
13. J.E. Fromm: Numerical calculation of the fluid dynamics of drop-on-demand jets. *IBM J. Res. Dev.* **28**, 322–333 (1984).
14. N. Reis and B. Derby: Ink jet deposition of ceramic suspensions: Modeling and experiments of droplet formation. *Mater. Res. Soc. Symp. Proc.* **625**, 117 (2000).
15. N. Reis, C. Ainsley, and B. Derby: Ink-jet delivery of particle suspensions by piezoelectric droplet ejectors. *J. Appl. Phys.* **97**, 094903 1-6 (2005).
16. H. Bredereck, B. Föhlisch, R. Franz, G. Grahe, P. Petranyi, K. Posselt, H. Sigel, E. Tag, and W. Wirths: About CH-active polymerisation initiators. XIII. Polymerisations and polymerisation initiators. *Die Makromolekulare Chemie* **92**, 70–90 (1966).
17. R. Hecht and M. Ludsteck: Initiator system for acid dental formulations, WO 02092023 (2002).
18. I. Yuji, K. Yoshinori, and K. Toru: Polymerization initiator composition controlling polymerization at interface and curable composition containing same, EP0480785 (1992).
19. B.W. Brooks: Free-radical polymerization: Suspension. In *Handbook of Polymer Reaction Engineering*, Th. Meyer and J. Keurentjes, eds.; Wiley-VCH Verlag GmbH: Weinheim, Germany, 2008, pp. 213–247.
20. N.K. Kalfoglou and C.E. Chaffey: Effects of extrusion on the structure and properties of high-impact polystyrene. *Polym. Eng. Sci.* **19**, 552–557 (1979).

https://doi.org/10.1557/jmr.2014.137 Published online by Cambridge University Press